Paleoceanography and Paleoclimatology®

AGU ADVANCING EARTH AND SPACE SCIENCE

RESEARCH ARTICLE
10.1029/2021PA004223

Key Points:

- Marine record documents decadal- to millennial-scale fluctuations of monsoonal rainfall in eastern South America during the past 5,000 years
- Precipitation variability was caused by antiphased shifts of South Atlantic Convergence Zone and South American Low-Level Jet
- Changes in oceanic overturning strength mediate transfer of high-northern-latitude climate disturbances into southern hemisphere tropics

Supporting Information:

Supporting Information may be found in the online version of this article.

Correspondence to:

A. Bahr,
andre.bahr@geow.uni-heidelberg.de

Citation:

Bahr, A., Kaboth-Bahr, S., Jaeschke, A., Chiessi, C., Cruz, F., Carvalho, L., et al. (2021). Late Holocene precipitation fluctuations in South America triggered by variability of the North Atlantic overturning circulation. *Paleoceanography and Paleoclimatology*, *36*, e2021PA004223. https://doi.org/10.1029/2021PA004223

Received 13 JAN 2021
Accepted 24 AUG 2021

Late Holocene Precipitation Fluctuations in South America Triggered by Variability of the North Atlantic Overturning Circulation

A. Bahr[1], S. Kaboth-Bahr[1,2], A. Jaeschke[3], C. Chiessi[4], F. Cruz[5], L. Carvalho[6], J. Rethemeyer[3], E. Schefuß[7], P. Geppert[1], A. L. Albuquerque[8], J. Pross[1], and O. Friedrich[1]

[1]Institute of Earth Sciences, Heidelberg University, Heidelberg, Germany, [2]Institute of Earth Sciences, University of Potsdam, Potsdam-Golm, Germany, [3]Institute of Geology and Mineralogy, University of Cologne, Cologne, Germany, [4]School of Arts, Sciences and Humanities, University of São Paulo, São Paulo, Brazil, [5]Institute of Geosciences, University of São Paulo, São Paulo, Brazil, [6]Department of Geography and Earth Research Institute, University of California, Santa Barbara, CA, USA, [7]MARUM—Center for Marine Environmental Sciences, University of Bremen, Bremen, Germany, [8]Departamento de Geoquímica, Universidade Federal Fluminense, Niterói, Brazil

Abstract Historic droughts document the strong spatio-temporal variability of the South American Monsoon System, which currently provides more than two thirds of the rainfall in tropical South America. The drivers of this variability have remained not well understood due to the lack of continuous, high-resolution paleorecords, especially from the more arid regions of tropical South America. Here we present a novel record of moisture availability across eastern South America for the past ~5,000 years from a sediment core retrieved off eastern Brazil. We document distinct decadal- to millennial-scale spatial shifts of major atmospheric convection centers that caused increasingly pronounced droughts in eastern South America over the past ~2,000 years. These fluctuations were triggered by climate anomalies in the high northern latitudes and propagated into equatorial latitudes via fluctuations in North Atlantic Overturning Circulation strength. As global warming is expected to decrease oceanic overturning due to enhanced meltwater input into the North Atlantic while at the same time reducing precipitation over eastern South America, an increasing risk for long-lasting droughts can be expected for this region, posing severe socio-economic challenges.

1. Introduction

The South American Monsoon System (SAMS) is the dominant hydroclimatic feature in tropical South America as it determines the amount and spatial distribution of rainfall over large portions of the continent (Vera et al., 2006). SAMS-induced rainfall provides the water resources for millions of people and is crucial for both agriculture and hydroelectric power generation, the latter being the most important electricity source in South America (Hunt et al., 2018). A strong spatiotemporal variability of the SAMS is manifested historically in dry spells that lasted several years and caused tens of thousands of fatalities over the past four centuries (Coelho et al., 2016; Marengo et al., 2017; Tomasella et al., 2019). Future climate-change scenarios predict an increase in aridity over large parts of South America in response to global warming (IPCC, 2021; Marengo & Bernasconi, 2015; Marengo et al., 2017). In light of the severe societal impact of such droughts, it is crucial to constrain the natural variability of the SAMS and to understand the underlying forcing mechanisms. Such knowledge will help to better assess the impact of future climate change on water availability in South America (Erfanian et al., 2017; Hunt et al., 2018; IPCC, 2021), particularly over decadal to centennial time scales.

An important component of the SAMS is the South Atlantic Convergence Zone (SACZ), which forms a convective band extending from the Amazon Basin across central Brazil to the western South Atlantic Ocean (Carvalho, 2020; Carvalho et al., 2004; Figure 1a). The SACZ is fueled by a cyclonic circulation over eastern South America that funnels moisture from the Amazon Basin into southeastern Brazil (Bombardi et al., 2014). Regions south of the SACZ receive substantial precipitation from the South American Low-Level Jet (SALLJ), which transports moisture from the Amazon Basin along the eastern slope of the Andes to southeastern South America (i.e., mainly the La Plata Basin and southern Brazil; Jones & Carvalho, 2018; Vera et al., 2006). Climatological data of the past century demonstrate that a strong (weak) SACZ goes

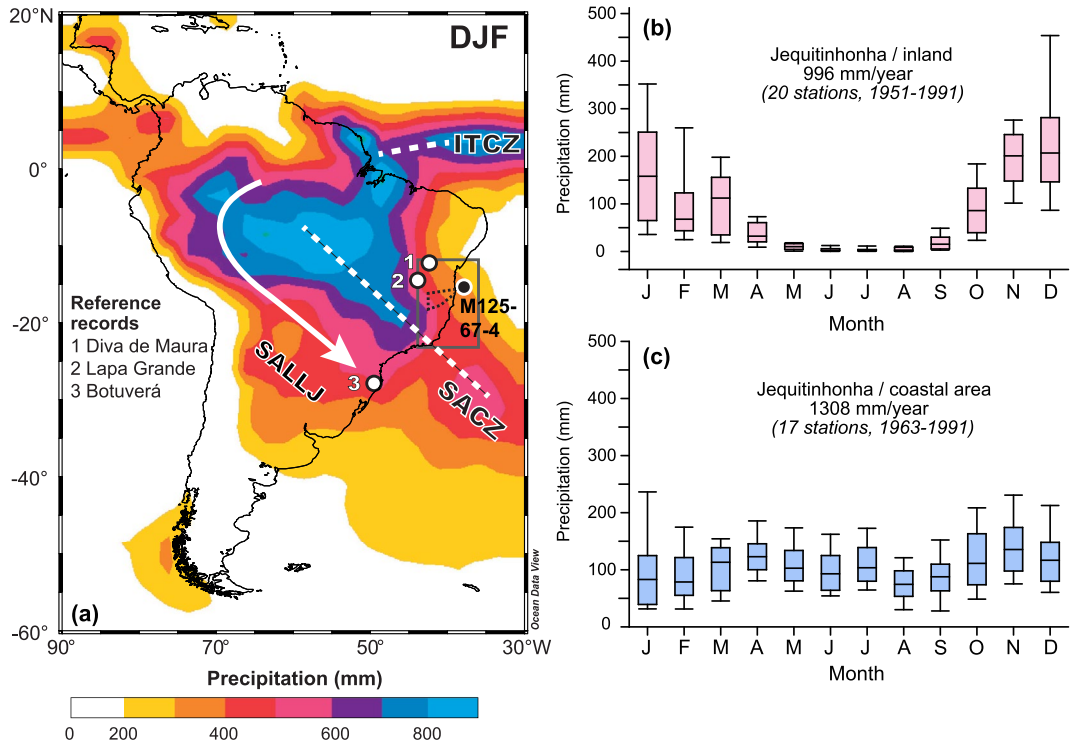

Figure 1. (a) Map showing mean precipitation in eastern South America from December to February (DJF) between 1979 and 2000 (Climate Prediction Center Merged Analysis). The positions of marine core M125-67-4 (black dot) and other sites discussed in the text (white dots) are indicated: (1) Diva de Maura Cave (Novello et al., 2012), (2) Lapa Grande Caves (Stríkis et al., 2011), and (3) Botuverá Cave (Bernal et al., 2016). The black dashed line marks the Jequitinhonha River catchment, the white stippled line depicts the mean position of the South Atlantic Convergence Zone (SACZ), the white arrow denotes the South American Low-Level Jet (SALLJ). Gray rectangle denotes area shown in Figure 2. Right panel: Hydrological cycle in the Jequitinhonha River catchment. Box-Whisker plots of precipitation variability in the catchment of the Jequitinhonha River for the (b) mountainous inland region (area A in Figure 2) and (c) coastal regions (area B in Figure 2). Whiskers indicate 10 and 90 percentiles, the box is defined by the lower and upper quartiles, and the line in the center of the box represents the median. The data were retrieved from the KNMI Climate Explorer (http://climexp.knmi.nl).

along with a weak (strong) SALLJ, which induces a distinct spatio-temporal dipole over southeastern South America on annual to decadal time scales (Jones & Carvalho, 2018; Liebmann et al., 2004; Vera et al., 2006).

Available records of SAMS intensity suggest that its orbital-scale variability was influenced by insolation forcing generating a spatially complex precipitation pattern (Baker & Fritz, 2015; Deininger et al., 2019; Novello et al., 2018). Generally, high austral summer insolation leads to a heating of the continent relative to the ocean, thereby promoting convective rainfall over much of South America (Baker & Fritz, 2015; Cruz et al., 2005; Hou, Bahr, Raddatz, et al., 2020). At the same time, high austral summer insolation enhances the subsidence of moisture-barren air over northeastern Brazil (i.e., the Nordeste Low), which results in an E-W precipitation dipole across the continent (Cruz et al., 2009; Figure 1). Paleorecords of the past ~1 kyr allude to the potential impact of northern high-latitude climate fluctuations on SAMS intensity at centennial time scales, particularly in regions affected by both the SACZ and the SALLJ (Campos et al., 2019; Deininger et al., 2019; Jones & Carvalho, 2018; Novello et al., 2018). However, as shown by an increasing number of proxy data, the impact of such short-term fluctuations on the spatial precipitation distribution within the SAMS domain is highly complex. This complexity has led to partly conflicting interpretations, arguing either for major shifts of the position of the convective centers over (sub)tropical South America (e.g., Bernal et al., 2016; Novello et al., 2018) or in favor of their contraction/expansion without a geographic displacement (e.g., Campos et al., 2019; Deininger et al., 2019; Utida et al., 2019). A leading role of transmitting high-northern-latitude climate disturbances into low latitudes has been attributed to changes in oceanic heat transport via its impact on the inter- and intrahemispheric temperature distribution (e.g., P.

Chang et al., 1997; Hou, Bahr, Schmidt, et al., 2020; Seidov & Maslin, 2001). Such changes influence the large-scale atmospheric circulation across the South Atlantic Ocean and South America, which is, for example, documented by a southward shift and/or expansion of the Hadley Cell during high-northern-latitude cold phases (Asmerom et al., 2020; Vuille et al., 2012). However, the exact mechanisms of how changes in oceanic heat transport influence precipitation amount and distribution within the region influenced by the SAMS are still not well constrained. This is an important shortcoming, because deciphering the sensitivity of the South American hydrological cycle to high-latitude forcing is crucial for mitigating the potential consequences of global warming (IPCC, 2021). This major shortcoming is at least in part due to the inability even of state-of-the-art numerical models to reliably simulate precipitation over the SAMS domain (Rojas et al., 2016).

To reconstruct the natural dynamics of moisture availability in eastern South America during the past ~5 kyr and to identify its driving forces, we used (a) bulk-sediment K/Al ratios based on X-ray fluorescence (XRF) core scanning combined with estimates of the mineralogical composition of the sediment determined via X-ray diffractometry (XRD) and (b) stable hydrogen isotopes (δ^2H) of plant waxes deposited in the sediment. The K/Al proxy for water availability is based on the rationale that increased precipitation enhances chemical weathering and promotes the release of more soluble elements such as potassium from soils in the dissolved phase (Tian et al., 2011; Yarincik et al., 2000). Thus, intense chemical weathering leads to a depletion of K- over Al-bearing mineral phases, resulting in low K/Al ratios in the suspended sediment loads during wet periods (Tian et al., 2011; Yarincik et al., 2000; Zabel et al., 2001). To further ground-truth the K/Al ratio as a proxy for continental hydroclimatic change we obtained an hydrogen-isotope record (δ^2H) on long-chain *n*-alkanes, which are constituents of the protective wax layer of terrestrial higher plants (Eglinton & Hamilton, 1967). Their δ^2H composition (δ^2H) reflects predominantly isotopic changes in rainfall (Sachse et al., 2012) overprinted by secondary changes due to upstream hydrological processes during atmospheric moisture transport (H. K. Chang et al., 2020; dos Santos et al., 2019), evapotranspiration (Kahmen, Hoffmann, Schefuß, et al., 2013; Kahmen, Schefuß, & Sachse, 2013b), and vegetation type (Sachse et al., 2012). In tropical areas, the isotopic composition of precipitation is mainly governed by rainfall amount (Dansgaard, 1964). We thus interpret our δ^2H record to be mainly associated with changes in the isotopic composition of precipitation (Sachse et al., 2012; Schefuß et al., 2005), with more depleted values indicating higher rainfall intensity and vice versa.

When put into spatial context with other paleo-precipitation archives, and complemented by observational and numerical model data, our records demonstrate that precipitation variability in eastern South America was highly sensitive to high-northern-latitude climate anomalies, pointing towards increasing risks of prolonged hydroclimatic extremes in the near future.

2. Climatology and Geology of the Jequitinhonha Catchment

The Jequitinhonha River is ~1,100 km long and drains an area of ~70,300 km^2. The vast majority of its catchment lies within the mountainous hinterland of eastern Brazil with relatively low annual rainfall of ~700–1,000 mm yr^{-1} (Figures 1a and 2; Xie & Arkin, 1997). Here, rainfall is strongly concentrated during austral summer when the SACZ is fully developed, while the long dry season lasts from April to September (Figure 1b). The coastal region, however, receives moisture advected by shoreward winds during austral winter and thus experiences more evenly distributed annual rainfall (~1,000–1,300 mm/yr) with no distinct dry season (Figure 1c; Grimm, 2011). Because the coastal region represents a small portion of the Jequitinhonha catchment, changes in the amount and composition of the sedimentary load delivery by the Jequitinhonha River to our study site predominantly reflect SACZ-influenced moisture availability in central-east Brazil.

The source of suspended sediments transported by the Jequitinhonha River lies in the Serra do Espinhaço in the State of Minas Gerais. It crosses the Precambrian basement of the São Francisco Craton and the Cenozoic coastal sediment deposits connected to the Araçuaí Fold Belt (CPRM—Serviço Geológico do Brasil, 2003a, 2003b). The lithotypes eroded in the upper part of the drainage basin consist of schists, migmatites and other metamorphites, quartzites, and granites, while the lower part mainly comprises sandstones (Tintelnot, 1995).

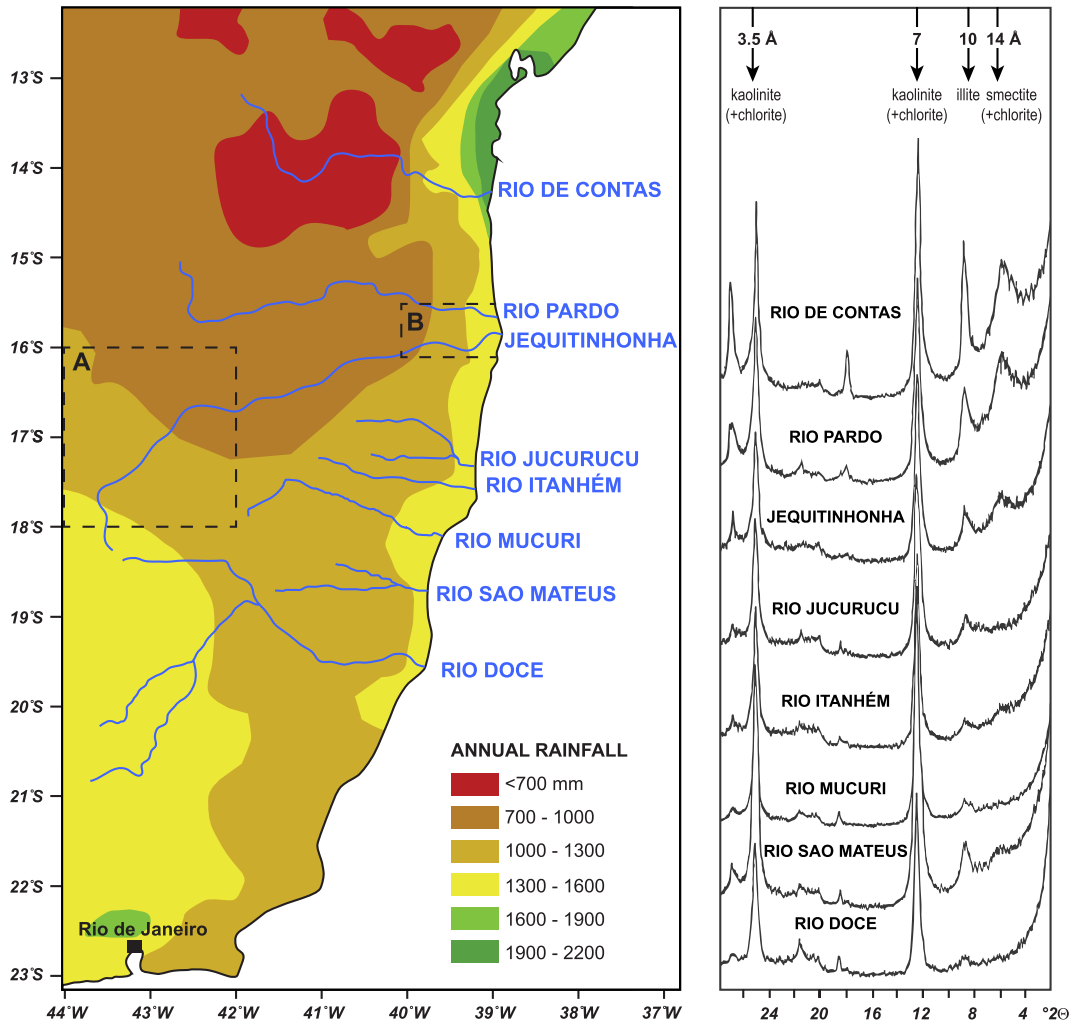

Figure 2. Moisture availability and weathering intensity in eastern Brazil reflected by clay mineralogy. Left panel: Annual rainfall distribution in eastern Brazil (modified after Alvares et al., 2013; Marengo & Bernasconi, 2015) and rivers sampled for clay mineralogical analyses by Tintelnot (1995). Dashed rectangles indicate areas used to calculate annual precipitation distribution in Figure 1. Right panel: X-ray diagrams of the clay fraction (<2 μm, Mg^{++}- and K^{+}-saturated) from eastern Brazilian river sediments (Tintelnot, 1995). Positions of kaolinite, illite, and chlorite are indicated by arrows with the respective lattice spacing in Å. From north to south the increasing dominance of kaolinite over other clay minerals reflect the increasing mean annual rainfall.

The intimate link between moisture availability and weathering intensity in eastern Brazil is illustrated by the comparison of mean annual precipitation and the mineralogical composition of suspended river load (Tintelnot, 1995) (Figure 2). As expected, top soils and thus suspended sediments of rivers draining the less humid northern portion of eastern Brazil contain considerable amounts of weathering-sensitive minerals such as illite and smectite (e.g., the Contas River; Figure 2), in contrast to the near-exclusively kaolinite-dominated clay-mineral assemblage of rivers located in the more humid south (e.g., the Doce River). The suspended sediments of the Jequitinhonha River are at an intermediate level with clearly detectable illite and smectite (Figure 2). However, the dominant mineral phase is kaolinite, illustrating the strong chemical weathering conditions in this drainage basin. The congruence of precipitation amount and clay-mineral composition illustrates that climate is the foremost factor determining the strength of weathering-sensitive versus residual phases in river-suspended sediments in eastern Brazil (Tintelnot, 1995).

3. Materials and Methods

3.1. Coring and Sampling

Gravity core M125-67-4 (15°16.964′ S, 038°54.801′W, 28 m water depth) has been retrieved during R/V Meteor Expedition M125 in April 2016, 57 km northeast of the mouth of the Jequitinhonha River (Bahr et al., 2016). The obtained sediments consist dominantly of brownish silt to sandy silt with occasional macroscopic mollusk shells (gastropods and bivalves). The sediments transported by the Jequitinhonha River record the moisture availability at the northeastern boundary of the region currently affected by the SACZ (Figure 1). Hence, the core site is ideally located to reconstruct both the strength and spatial variability of the SAMS during its peak season (DJF).

Upon retrieval, cores were split into 1 m segments and opened onboard. The archive half was used for XRF scanning, while the working half was sampled for mineralogical analysis (mean sampling spacing: 6.5 cm, $n = 77$). Selected samples ($n = 8$) have been additionally retrieved for stable-isotope analyses on long-chain *n*-alkanes. Sample positions for stable isotope analyses align with extreme values in the ln(K/Al) record obtained by XRF core scanning (see Section 5).

3.2. XRF Core Scanning

Non-destructive XRF scanning was performed with an AVAATECH XRF Core Scanner IV at the Institute of Earth Sciences, Heidelberg University. Scanning was carried out in 1-cm intervals on the split core with a slit size of 12-mm down-core and 10-mm cross-core. Two runs were performed for each depth with the following settings for tube voltage, current and filter: 10 kV, 100 μa, no filter and 30 kV, 500 μa, Pd-filter. Sampling time was set to 10 s and scanning took place directly at the split core surface. The split core surface was covered with a 4 μm thin SPEXCerti Prep Ultralene1 foil to avoid contamination of the measurement unit and desiccation of the sediment. The reported data have been acquired using a Canberra X-PIPS Silicon Drift Detector (SDD; Model SXD 15C-150-500) with 150 eV X-ray resolution and the Canberra Digital Spectrum Analyzer DAS 1000 with a rhodium (Rh) target material. Raw data spectra were processed by the analysis of X-ray spectra by the Iterative Least Square software (bAXIL) package from Canberra Eurisys. Relative standard deviations for Al and K are 1.1% and 1.0%, respectively.

3.3. XRD Analyses

The sample preparation consists of drying and powdering the samples, which was performed with a FRITSCH "Pulverisette" planetary mill. XRD measurements were carried out using a Bruker D8 ADVANCE Eco diffractometer (40 kV, 25 mA) with a Cu Ka diode at the Institute of Earth Sciences, Heidelberg University. The samples were measured with an angular range of 2θ from 5° to 70° in 0.02 increments (3,338 steps per sample) for 1 s per step. The XRD data were semi-quantitatively evaluated using the "DIFFRAC. SUITE EVA" software.

3.4. Lipid Biomarker Analysis

Freeze-dried sediment samples (~20 g) were ultrasonically extracted (3×) using a mixture of dichloromethane (DCM) and methanol (2:1, v/v). The extracts were combined and the bulk of the solvent subsequently removed by rotary evaporation under vacuum. The resulting total lipid extracts were separated into apolar (with *n*-hexane), ketone (with DCM), and polar (with DCM:methanol 1:1) fractions using activated silica gel chromatography. The apolar fractions containing *n*-alkanes were further separated into saturated and unsaturated compounds over small columns filled with $AgNO_3$ coated silica gel (10% w/w) using *n*-hexane and DCM, respectively.

Compound-specific stable hydrogen isotope (δ^2H) analysis of long chain *n*-alkanes was performed on a Trace GC coupled via a pyrolysis reactor to a ThermoFisher Scientific MAT 253 mass spectrometer. The GC was equipped with a 30 m × 0.25 mm column (Restek Rxi-5 ms, film thickness: 1.0 μm) and He was used as the carrier gas. The fractions were injected via a PTV injector at 40°C and then transferred to the GC column. The GC temperature was programmed to increase from 120°C (2 min hold) to 200°C at 30°C/min and

Table 1
Accelerator Mass Spectrometry (AMS) ^{14}C Ages Performed on Core M125-67-4, Including 2σ Error

AMS-Lab-ID	Depth (cm)	Number of shells	^{14}C age (year BP)	Calibrated age (a)
MAMS 30981	100	2	617 ± 19	195 ± 84
BETA 487707	130	14	1,280 ± 30	623 ± 144
BETA 487708	170	19	1,550 ± 30	873 ± 177
MAMS 30982	200	1	2,819 ± 25	2,309 ± 222
BETA 493295	210	18	2,750 ± 30	2,220 ± 209
MAMS 30983	297	1	3,171 ± 23	2,748 ± 200
BETA 487709	340	23	3,610 ± 30	3,276 ± 198
MAMS 30984	391	1	4,123 ± 22	3,917 ± 216
COL4227.1.1	417	1	4,668 ± 51	4,635 ± 223
BETA 487710	480	14	4,840 ± 30	4,851 ± 235

Note. Calibration was done using the CALIB 8.2 software (Stuiver et al., 2020) (http://calib.org/calib/calib.html). Dating substrate were bivalve shells from the fraction <1 cm. Laboratory codes: BETA—Beta Analytic Inc.; COL—University of Cologne; MAMS—Curt Engelhorn Centre for Archeometry Mannheim, Germany.

then at 4°C/min to 320°C (held 12.3 min). H_2 was used as reference gas and δ^2H values are given in ‰ relative to Vienna Standard Mean Ocean Water. The H_3 factor monitored on a daily basis was 5.09 ± 0.02 during analysis. An external standard mixture (16 *n*-alkanes and squalane) with known δ^2H values was analyzed repeatedly every six runs, yielding a long-term mean standard deviation of <3‰ and a mean deviation of <1‰ from reference values. All samples were analyzed in duplicate with an average standard deviation of 2‰. As *n*-C_{29} alkane is produced by all terrestrial higher plants (Bush & McInerney, 2013; Diefendorf & Freimuth, 2017) and could be measured most reliably (mean concentration: 34% of all *n*-alkanes), we have focused on the δ^2H data from this compound.

3.5. Statistical Analyses

Correlations (based on Pearson's *r*) between different data sets were performed using the MonteCarlo-based "SurrogateCor" function implemented in R (Meyers, 2014) with 1,000 iterations. This function was particularly designed for comparison of data sets on different time or depth-scales.

3.6. Spectral Analysis

Spectral analysis of the ln(K/Al) ratio was performed on the detrended, non-interpolated data using REDFIT (Schulz & Mudelsee, 2002) implemented in the program PAST 3.15 (Hammer et al., 2001) using a Welch-window (oversampling = 4, window width = 4). Wavelet and cross-wavelet analyses were performed on detrended and interpolated data with the wt and xwt functions, respectively, which are implemented in the "biwavelet" package in R (Gouhier et al., 2019) using a Morlet wavelet.

4. Chronostratigraphy

Ten Accelerator Mass Spectrometry (AMS) ^{14}C analyses were performed on Core M125-67-4 (Table 1) using bivalve shells, preferably of juvenile forms with translucent shells to avoid deep endobenthic specimens. Dating was carried out at the AMS ^{14}C facilities of Beta Analytic Inc, USA, the University of Cologne, Germany, and the Curt Engelhorn Centre for Archeometry, Germany. The age model was constructed using the median values provided by the Bayesian program BACON implemented in R (Blaauw & Christen, 2011) with the MARINE20 data base and a local reservoir age of $\Delta R = 58 \pm 53$ years (Alves et al., 2015). Resulting sedimentation rates vary mostly between 20 and 160 cm/kyr indicating substantial variations in sediment input of the Jequitinhonha River over the past ~5,000 years (Figure 3). Exceptionally high sedimentation rates of ~510 cm/kyr have been reconstructed for the past ~200 years, likely due to anthropogenically induced erosion by deforestation and cattle grazing (Ribeiro et al., 2009). To avoid any anthropogenic bias, we therefore excluded the 0–200-year interval from our study.

5. Results

The ln(K/Al) ratios of Core M125-67-4, reflecting changes in the weathering state in the Jequitinhonha catchment, vary between 0.5 and 1.1 (Figure 4b). An exception is constituted by the last ~200 years with values of up to 1.3. However, due to the presumed anthropogenic bias we excluded this interval from further discussion (see Section 4). Minimum ln(K/Al) values around 0.5, indicating wet conditions in the catchment of the Jequitinhonha, occur at the base of the core at ~5 ka followed by an increase to values of ~0.9 between 4.5 and 4.4 ka and a subsequent return to minimum values at ~3.2 ka. Afterward, ln(K/Al) ratios increase progressively with an abrupt shift at ~2.0 ka to a level of ~0.9, suggesting a decline in continental

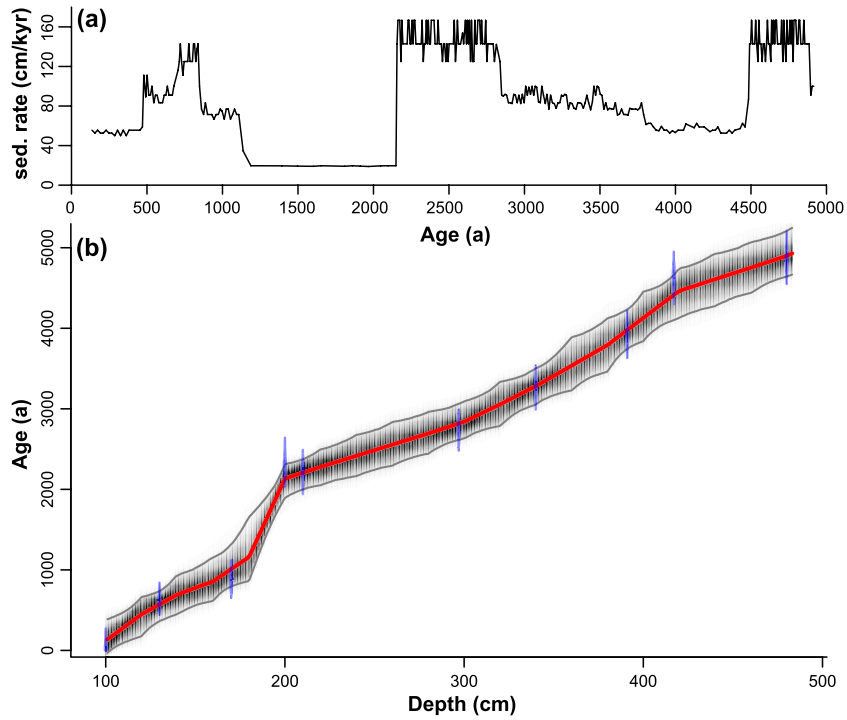

Figure 3. Age model for Core M125-67-4 as derived from radiocarbon dating. The Bayesian program BACON (Blaauw & Christen, 2011) was used in order to construct (a) sedimentation rates and (b) the age-depth relation (median: red line; gray line: 2σ envelope). Note that the last ~200 years have been excluded from the study due to potential anthropogenic overprint.

precipitation. The ln(K/Al) record remains on this level with two ~200-year-long excursions to lower values (i.e., wetter conditions) centered at ~0.9 and ~0.6 ka.

The long-term variability of ln(K/Al) is well reflected by the lower-resolution record of the microcline versus kaolinite ratio (Figure 4a). Both parameters are significantly correlated ($r^2 = 0.28$, $p < 0.05$; on detrended data, excluding the upper 100 cm), corroborating the assumption that the ln(K/Al) ratio basically reflects relative changes of K-bearing feldspars and mica versus K-depleted aluminosilicates such as kaolinite.

The δ^2H values (Figure 4c) display a long-term trend from −154‰ at 4.4 ka toward less depleted values of −147‰ at 0.6 ka, suggesting a general trend toward drier conditions over the past 5 kyr, in line with evidence from the ln(K/Al) record.

6. Discussion

6.1. Monsoonal Variability in Eastern Brazil

The ln(K/Al) record of Core M125-67-4 documents a pronounced SAMS variability in eastern Brazil during the past ~5 kyr on millennial to decadal time scales (Figures 4b and 5b). The ability of the employed ln(K/Al) ratio to reliably reflect the weathering state in the Jequitinhonha River catchment is supported by the similarity of its distribution with that of the weathering-sensitive feldspar/kaolinite ratio in Core M125-67-4 (Figure 4a). The general trend toward drier conditions over the past 5 kyr as indicated by the ln(K/Al) record is also reflected by the δ^2H record (despite diverging excursions between both records at 4.4 and 0.6 ka), corroborating the robustness of the retrieved climatic signal. This long-term trend to drier conditions in the northern portion of eastern Brazil agrees with increasing austral summer insolation (Figure 5a), which leads to an intensification of the Nordeste Low and thus higher aridity in the Jequitinhonha catchment (Chiessi et al., 2021; Cruz et al., 2009).

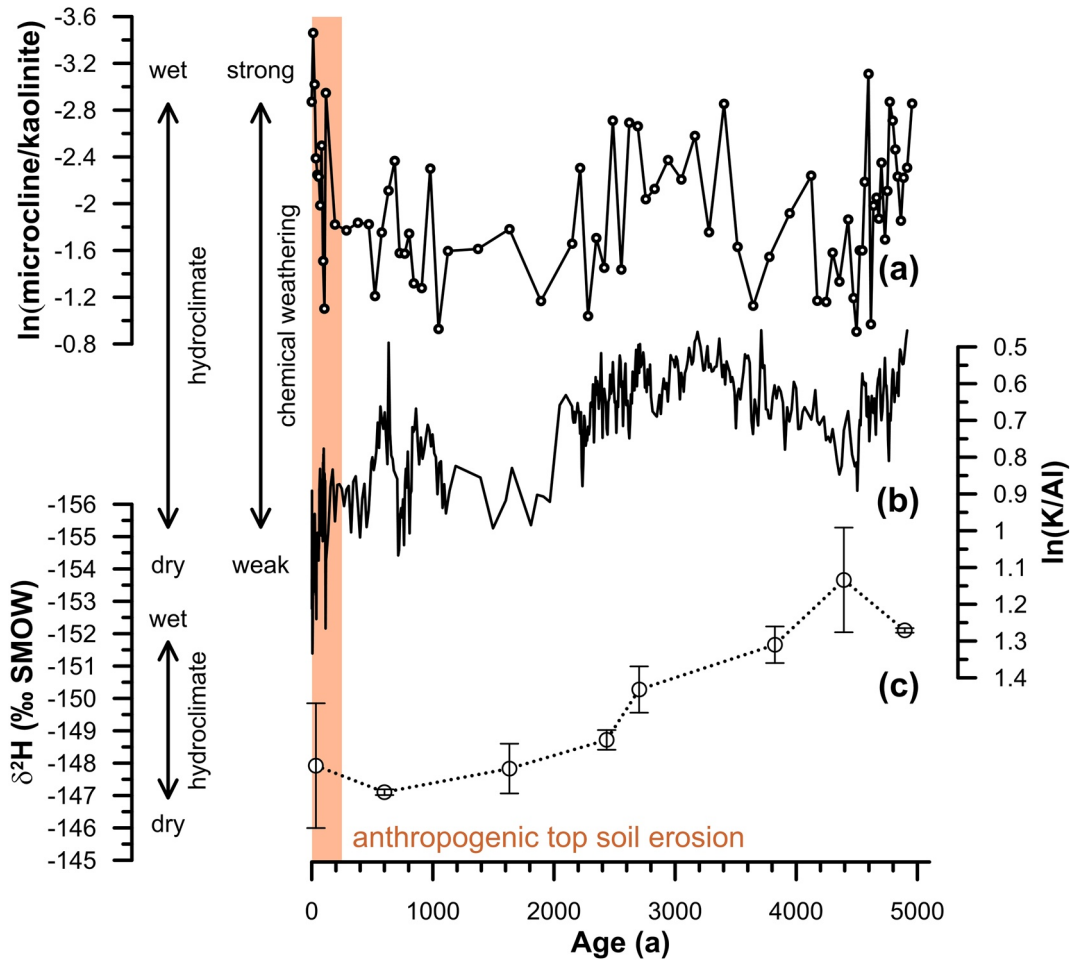

Figure 4. Inorganic and organic geochemical proxies obtained on Core M125-67-4. (a) Downcore distribution of microcline (K-bearing) versus kaolinite (K-free) ratios, interpreted to primarily represent chemical weathering intensity in the hinterland and (b) sedimentary ln(K/Al) values of Core M125-67-4 reflecting the distribution of microcline versus kaolinite. (c) δ^2H of terrigenous plant waxes.

A general trend to drier conditions at least over the past 2 ka is also registered in speleothem $\delta^{18}O$ records from the neighborhood of the Jequitinhonha catchment (Diva de Maura and Lapa Grande Caves, Figures 6a and 6b; Novello et al., 2012; Stríkis et al., 2011). While the long-term trend also shows some agreement for the older parts of the records, for example, between Lapa Grande and Core M125-67-4 from 5 to 4 ka (Figure 6), the speleothem $\delta^{18}O$ includes more distinct decadal-scale fluctuations that are not apparent with a similar large amplitude in the ln(K/Al) data of Core M125-67-4 (Figure 6c). These differences in signal amplitude are likely due to different proxy sensitivities as soil weathering processes will buffer fluctuations acting on decadal or shorter time scales. In addition, signal mixing by bioturbation will smooth out high-frequency climate variability in Core M125-67-4 that is well preserved in speleothem records. The $\delta^{18}O$ signal of speleothems and the δ^2H signal of plant waxes in Core M125-67-4 are further sensitive to shifts in moisture sources that are irrelevant for soil weathering. The retrieved ln(K/Al) signal, on the other hand, might be influenced by changes in vegetation cover that enhanced or prevented topsoil erosion (cf. discussion in Section 4). Lastly, the ln(K/Al) record of Core M125-67-4 integrates over a relatively wide catchment area, while local effects are much more prone to influence speleothems records. Such local influences (even within a single cave) might also well explain some of the differences between the Diva de Maura and Lapa Grande $\delta^{18}O$ records.

However, even when considering proxy- or site-related biases and age-model uncertainties, the differences between both cave records and the ln(K/Al) data from Core M125-67-4 are substantial. This points at a

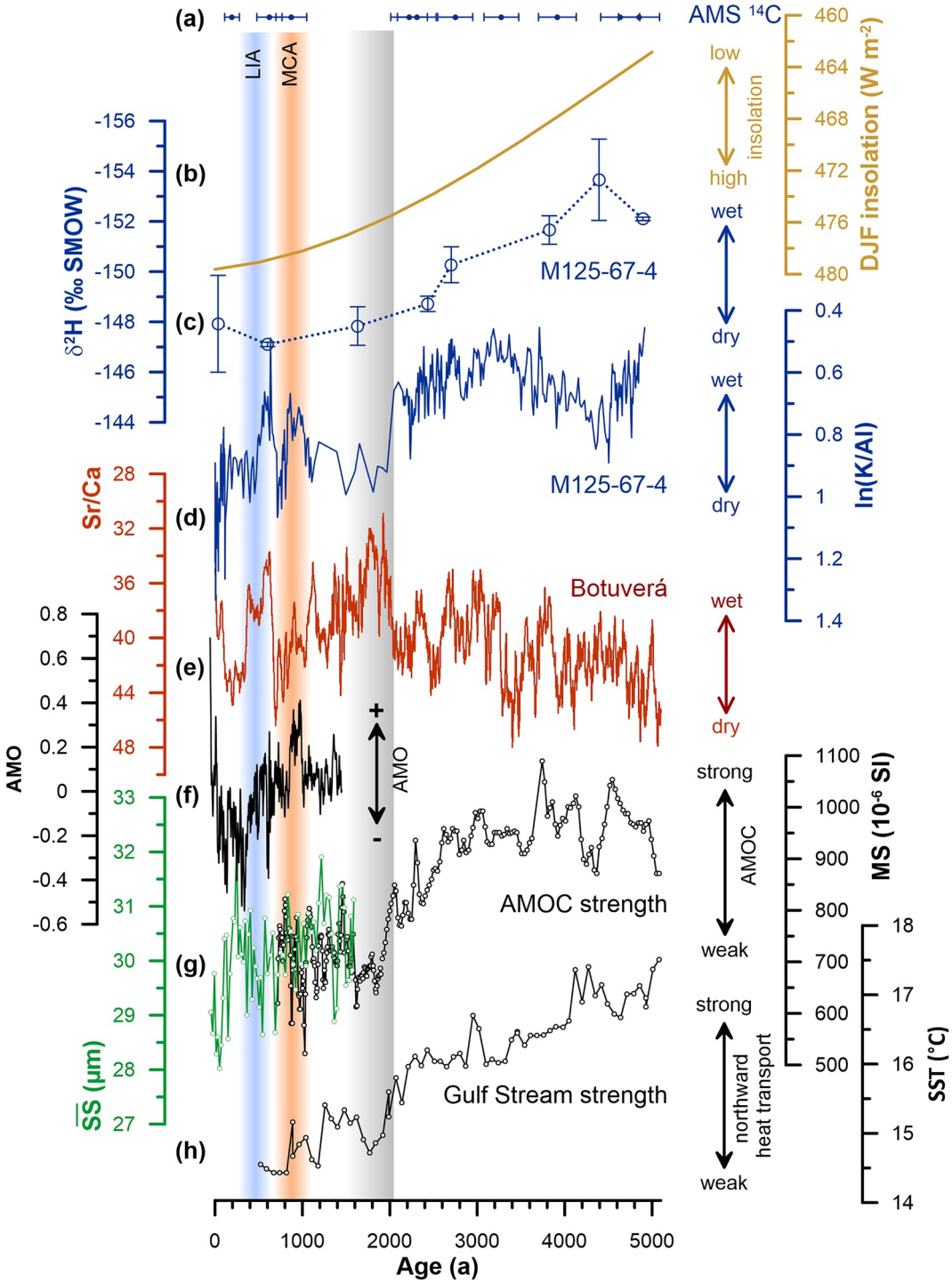

Figure 5. Changes in the hydroclimate of eastern Brazil, insolation, and oceanic circulation off the Brazilian coast during the past 5 kyrs. (a) Integrated austral summer insolation at 20°S (December, January, February—DJF; Laskar et al., 2004), (b) Accelerator Mass Spectrometry (AMS) ^{14}C ages, (c) sedimentary ln(K/Al), and (d) δ^2H of terrigenous plant waxes of Core M125-67-4 (eastern Brazil, this study) compared to (e) Sr/Ca of a Botuverá Cave speleothem (Bernal et al., 2016) from southeastern Brazil; (f) Atlantic Multidecadal Oscillation (AMO) index by Mann et al. (2009); (g) Atlantic Meridional Overturning Circulation (AMOC) strength inferred from magnetic susceptibility (MS, black line) at Gardar Drift (Kissel et al., 2013) representing the flow speed of the Islandic Overflow Water and sortable silt ($\overline{SS}$) from Core KNR-178-48JPC off Cape Hatteras reflecting Deep Western Boundary Current speed (green line) (Thornalley et al., 2018); (h) alkenone-based sea-surface temperatures (SST) from Core GGC19 (37°N, 75°W) (Sachs, 2007) indicating Gulf Stream strength; gray bar indicates the major shift of the South Atlantic Convergence Zone (SACZ) position commencing at 2.0 ka. Red and blue bars denote the Medieval Climate Anomaly (MCA) and the Little Ice Age (LIA), respectively.

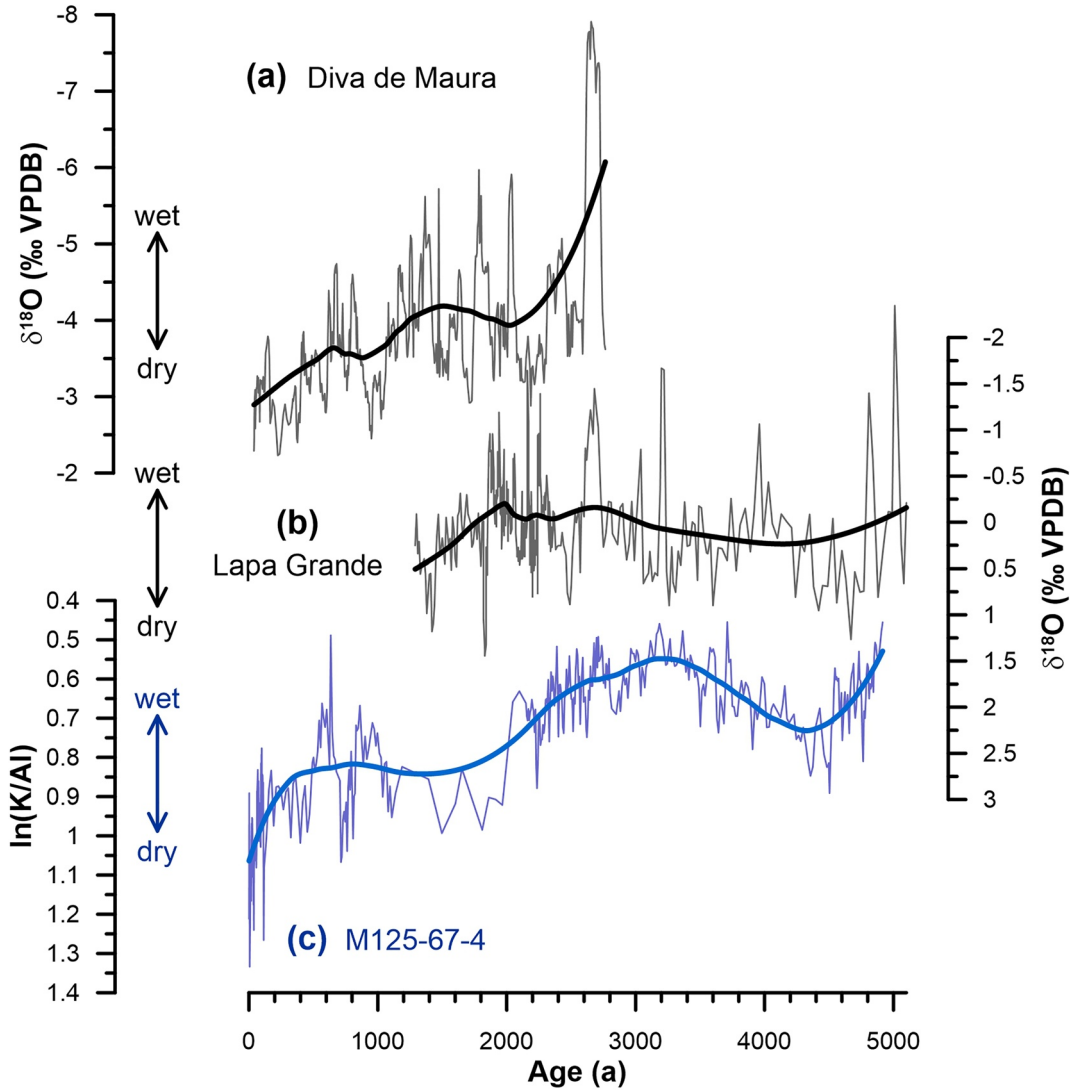

Figure 6. Reconstruction of moisture availability on core M125-67-4 in relation to speleothem records from central eastern Brazil: (a) Diva de Maura Caves (Novello et al., 2012), (b) Lapa Grande (Stríkis et al., 2011), and (c) sedimentary ln(K/Al) ratio from Core M125-67-4. For site locations, see Figure 1. Thick lines denote LOESS smoothing of the respective records to illustrate long-term trends (smoothing factors: 0.65 for Lapa Grande and Diva da Maura, 0.3 for Core M125-67-4). Note that $\delta^{18}O$ of speleothems are interpreted to predominantly reflect precipitation amount but might be biased by moisture source changes (Baker et al., 2005).

spatially complex precipitation pattern affecting the respective caves (Diva de Maura and Lapa Grande), which are located in a more continental and thus arid setting in central-eastern Brazil, differently from the more coastal and on average wetter Jequitinhonha catchment (Figures 1 and 2). As discussed in the following, the observed millennial- and centennial-scale variations in the proxy record from Core M125-67-4 are thus not uniform across eastern Brazil. We argue that this regional-scale spatial variability in precipitation has been largely produced by alternating variations in SACZ and SALLJ strength (Deininger et al., 2019; Novello et al., 2018).

6.2. Reconstructing Spatial Precipitation Shifts

The strong impact of SACZ and SALLJ dynamics on the precipitation distribution within the SAMS domain over the past 5 kyr becomes obvious from the comparison between the weathering-intensity record from Core M125-67-4 and the speleothem-based monsoonal rainfall record from Botuverá Cave in southeastern

Brazil (Figures 1 and 5). The record from Botuverá Cave is based on Sr/Ca ratios in the speleothem calcite that are primarily controlled by the recharge of the water table by monsoonal rainfall above the cave (Bernal et al., 2016; Cruz et al., 2007). High (low) Sr/Ca ratios correspond to dry (wet) conditions and are thus a direct measure of the on-site precipitation amount (Bernal et al., 2016). We selected the Sr/Ca record because available $\delta^{18}O$ data from Botuverá Cave have a lower temporal resolution and are also influenced by the upstream recycling history of atmospheric moisture in the wider SAMS domain (Bernal et al., 2016). Because Core M125-67-4 lies at the northeastern boundary of the SACZ, while Botuverá Cave receives precipitation from the southwestern sector of the SACZ and the SALLJ (Figure 1), both datasets are well suited to track the potentially opposing behavior of both components of the SAMS. Hence, if pronounced and alternating variations in SACZ and SALLJ strength occurred during the middle to late Holocene, these should have produced antiphased rainfall changes at Botuverá Cave compared to the Jequitinhonha catchment. Likewise, a synchronous behavior of both records would indicate that the SACZ and SALLJ were largely stable, and that the amount of moisture advection from the tropical Atlantic into the SAMS was the main factor responsible for the reconstructed humidity variations.

For the past 5 kyrs, the Sr/Ca record from Botuverá Cave and the ln(K/Al) record from Core M125-67-4 indeed exhibit periods of antiphasing on multi-millennial to centennial time scales (Figures 5a and 5e) such as between 2 and 1.3 ka when wetter conditions were established at Botuverá while the Jequitinhonha catchment became drier. Within age-model uncertainties, a similar antiphased behavior occurred during the Medieval Climate Anomaly (MCA; c. 950–1250 CE; Mann et al., 2009), when wet conditions at Core M125-67-4 (i.e., a strong SACZ) were opposed by dry conditions at Botuverá (i.e., a weak SALLJ). The subsequent interval between c. 1300 and 1470 CE, which comprises the early Little Ice Age (LIA; c. 1400–1700 CE; Mann et al., 2009), however, was expressed by wet conditions in both records. Although at the limit of the chronostratigraphic resolution of Core M125-67-4, this observation is in line with previous findings from speleothems in eastern Brazil that indicate an expanded SACZ domain (Campos et al., 2019) that gave rise to wet conditions across entire eastern Brazil. The later phase of the LIA was again accompanied by a dipole of dry conditions in the Jequitinhonha catchment and wet conditions at Botuverá (Figure 5). This dipole-like behavior between SACZ and SALLJ continued to fluctuate on centennial time scales between 500 and 200 years and is well documented by proxy evidence (Campos et al., 2019), in line with present-day hydroclimatic observations (Liebmann et al., 2004). Numerical model experiments using CMIP5 and PMIP3 simulations for the past millennium (Rojas et al., 2016) likewise generate an atmospheric dipole between northeast and southwest Brazil for the LIA and MCA, mimicking the spatial pattern revealed by proxy evidence. However, the signs of the anomalies in the precipitation dipole provided by the model ensemble mean are exactly opposite to that revealed by proxy evidence. This data-model mismatch is largely attributed to the intrinsic inability even of state-of-the-art models to reliably assess austral summer precipitation amount over South America and thus stresses the urgent need to improve the models' skill to reliably capture hydroclimatic changes over the continent (e.g., Rojas et al., 2016; Sierra et al., 2015; Siongco et al., 2014).

The reconfigurations of the SACZ and SALLJ during the LIA and MCA, typical high-northern-latitude climate phenomena (Mann et al., 2009), demonstrate a close link of SAMS dynamics to distant climate anomalies and suggest that a considerable fraction of the reconstructed precipitation variability in eastern South America was driven by high-northern-latitude forcing (Deininger et al., 2019; Novello et al., 2018). One way to explain this teleconnection could be via the influence of the El Niño-Southern Oscillation (ENSO), which is a dominant climate mode in South America (Cai et al., 2020; Grimm, 2003; Grimm & Tedeschi, 2009). In particular for the MCA, a dominance of La Niña-conditions has been inferred (Conroy et al., 2010; Mann et al., 2009) that causes more precipitation over northeastern Brazil and drier conditions in southeastern South America. However, while dry conditions in Botuverá Cave would be in line with prevailing La Niña during the MCA (see Figure S1), the Jequitinhonha catchment is situated in a rather ENSO-neutral area to the south of the major precipitation anomaly over northeastern Brazil that develops during La Niña events (or El Niño with the reverse sign, respectively) (Cai et al., 2020) (Figure S1). This indicates that ENSO might have played a role for modulating rainfall at Botuverá Cave. However, as discussed in the following, other processes likely dominated fluctuations in moisture availability in eastern Brazil as recorded in Core M125-67-4.

6.3. The Role of AMOC on Eastern South American Precipitation Variability

We argue that the propagation of high-latitude climate disturbances and associated changes in ocean circulation into the SAMS domain might have been accomplished via altering the strength of the Atlantic Meridional Overturning Circulation (AMOC). The proposed link between SAMS dynamics and AMOC variability is reflected by the good correlation between SACZ/SALLJ strength and published AMOC proxies (Figure 5). This connection is evident for the progressive aridification of the Jequitinhona catchment (indicating reduced SACZ activity) after ∼3 ka juxtaposed to increasingly humid conditions at Botuverá Cave (increased SALLJ strength) that developed parallel to a reduced Islandic Overflow Water production recorded at the Gardar Drift in the North Atlantic (Figure 5g; Kissel et al., 2013). Because Islandic Overflow Water is a major constituent of North Atlantic Deep Water, its reduced production decreased AMOC strength. This reduced deep-water formation, likely caused by enhanced freshwater input into the Arctic and Nordic Seas (Thornalley et al., 2018), decreased the northward interhemispheric heat transport (Broecker, 1998) and resulted in cooling of the North Atlantic as evidenced by declining sea-surface temperatures (SST) in the northwestern North Atlantic (Sachs, 2007; Figure 5h). In particular, the distinct and abrupt shift at ∼2 ka toward a weak SACZ and strong SALLJ was marked by a rapid decline in Islandic Overflow Water production and a distinct drop in the strength of the Gulf Stream (Figures 5g and 5h) reducing northward heat transport. The MCA, on the other hand, was characterized by a strong AMOC that correlated with a weak SALLJ and an active SACZ. During the LIA, the pattern of weak AMOC correlating to weak SACZ and strong SALLJ (and vice versa for strong AMOC) is less straight forward as the transitory drop of AMOC strength around 1450 CE occurred parallel to strong precipitation at Botuverá Cave and in the Jequitinhonha catchment, indicating a spatially expanded SACZ (Campos et al., 2019). Hence, the magnitude of AMOC change appears to have to cross a critical threshold to invoke the observed SACZ-SALLJ dipole. Notably, a similar precipitation dipole between eastern and southeastern South America became apparent in numerical model experiments applying an extreme freshwater hosing of 1 Sv (i.e., 10^6 m^3 s^{-1}) into the North Atlantic. In contrast, this dipole pattern only faintly developed when a weak hosing is prescribed (0.1 Sv; Parsons et al., 2014), although the poor spatial resolution (2° in longitude, 2.5° in latitude) of the applied model limits its exact comparison with the available proxy data. The presence of a threshold in overturning strength is in line with the observation that the good match of AMOC proxies with SACZ and SALLJ variability appears only after ∼3 ka (Figure 5) which might be due to a relative stability of the AMOC prior to 3 ka, when both AMOC proxies lack a common pattern and thus might rather reflect local signals. In addition, the increasing austral summer insolation and ensuing aridification in northeastern Brazil during the late Holocene (Figure 5) might have led to a greater sensitivity of the hydroclimate in this region to relatively small-scale variations in oceanic overturning.

Based on the above evidence, we argue that changes in AMOC strength could have reinforced the observed dipole-behavior between SACZ and SALLJ via altering the SST distribution in the Atlantic Ocean. Southwards shifts of the SACZ during phases of weak AMOC such as the LIA have been inferred to lead to more precipitation over southeastern South America (Novello et al., 2012, 2018; Vuille et al., 2012). However, recent compilations of paleo-precipitation records argue that the position of the SACZ was rather stable, but might have intensified and weakened alternatingly, potentially due to changes in heat distribution and atmospheric circulation over the (sub)tropical South Atlantic (Campos et al., 2019). We further explore SASM dynamics along this avenue and argue that two largely independent mechanisms, both modulated by AMOC, were responsible for the observed changes between wet and dry conditions in this area: the South Atlantic Dipole and the Atlantic Multidecadal Oscillation (AMO).

6.4. Influence of the South Atlantic Dipole and the AMO

The SST distribution in the South Atlantic is well documented to influence the precipitation distribution over (sub)tropical South America (Bombardi et al., 2014; Wainer et al., 2014, 2021). The SST pattern is manifested as the South Atlantic Dipole that is in a positive mode when the tropical South Atlantic surface warms anomalously relative to the extratropical South Atlantic (and vice versa for a negative South Atlantic Dipole; see Figure S2) (Venegas et al., 1997). Sufficiently highly resolved SST records are yet lacking to reconstruct South Atlantic SST variability during the past 5 kyrs. However, recent numerical model experiments using the ensemble mean of the Community Earth System Model Last Millennium Ensemble

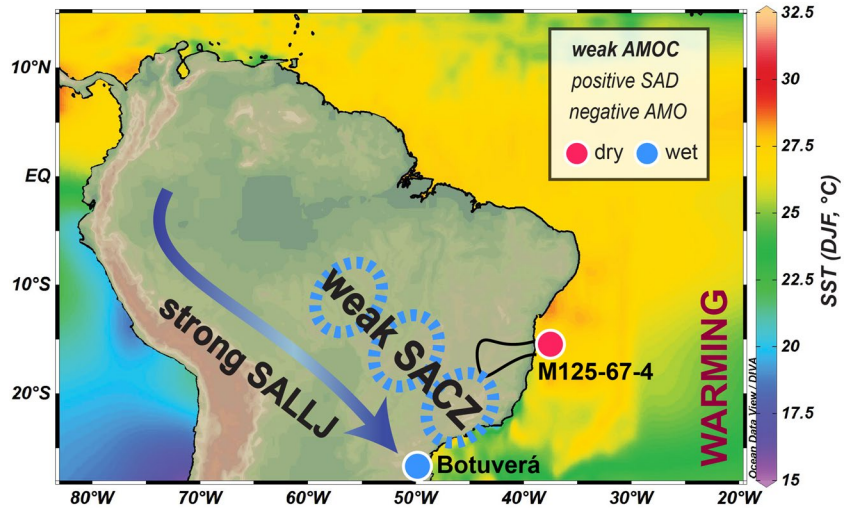

Figure 7. Schematic representation of Atlantic Meridional Overturning Circulation (AMOC) forcing acting upon the South American Summer Monsoon: Phases of weak AMOC such as during the Little Ice Age induced a positive South Atlantic Dipole (SAD) and negative Atlantic Multidecadal Oscillation (AMO), conditions that led to a weak South Atlantic Convergence Zone (SACZ) and a strong South American Low-Level Jet (SALLJ). This configuration induced a precipitation dipole over eastern South America, reflected by dry conditions in the catchment of the Jequitinhonha River (black line, recorded by Core M125-67-4; this study) and humid conditions at Botuverá Cave (Bernal et al., 2016). The opposite situation occurred during phases of strong AMOC, such as during the Medieval Climate Anomaly.

indicate that reconfigurations of ocean-surface currents in response to a transient weakening of the AMOC caused a cooling in the extratropical relative to the tropical South Atlantic (Marcello et al., 2019). Observational and reanalysis data (Bombardi et al., 2014) clearly show that the ensuing positive South Atlantic Dipole mode would have led to a strengthened SALLJ bringing more moisture toward Botuverá Cave, while reducing the frequency of cyclones and moisture advection toward central eastern Brazil (cf. Figure 7). The opposite mechanism operates during a negative South Atlantic Dipole mode that was active during phases of strong AMOC such as the MCA (Thornalley et al., 2018). This mechanism thus explains the enhanced precipitation over the Jequitinhonha catchment and drought at Botuverá Cave during high-northern-latitude warm phases (as, e.g., the MCA) and likewise the reverse situation during phases of weak AMOC such as between ~2.0 and 1.6 ka.

The South Atlantic Dipole-related impact on the precipitation distribution over eastern South America was likely amplified by the influence of the AMO on the SALLJ (Jones & Carvalho, 2018). The AMO is a major mode of multidecadal oscillation in the Earth's climate system that is in a positive (negative) phase when the high-latitude North Atlantic warms (cools) relative to its low-latitude counterpart. Climatological data indicate that the SALLJ is strong during negative AMO and thus enhances precipitation at Botuverá Cave (and vice versa for positive AMO) (Jones & Carvalho, 2018). During the MCA, the AMO was in a positive phase (Mann et al., 2009; Figure 5f) due to the pronounced high-latitude warming and strong AMOC, which is in line with the observed more arid phase at Botuverá Cave indicating a weak SALLJ (Figure 5). The plunge of the AMO into a distinctly negative index commencing at the late LIA, however, was again marked by a shift toward drier conditions in Botuverá Cave (Figure 5). This temporal pattern suggests a rather complex relation of the SALLJ to the long-term trend of AMO. Wavelet analysis of the Sr/Ca record from Botuverá Cave, on the other hand, suggests a persistent presence of AMO-related multi-decadal frequencies around 60 years throughout the record (Bernal et al., 2016), which might point to different sensitivities of southern Brazilian climate to AMO on different time scales.

To disentangle the potential imprint of AMO on precipitation variability in the Jequitinhonha catchment we have investigated the ln(K/Al) record of Core M125-67-4 by time series analyses (Figure 8). The power spectrum (Figure 8b) shows that the record comprises typical AMO-related periods in the range of ~60 years (Bernal et al., 2016; Chiessi et al., 2009). However, these periods are not continuously present throughout the record, but peak in the earlier parts around 4.3 and 3.6 ka, and potentially at 0.9 ka (cf. wavelet,

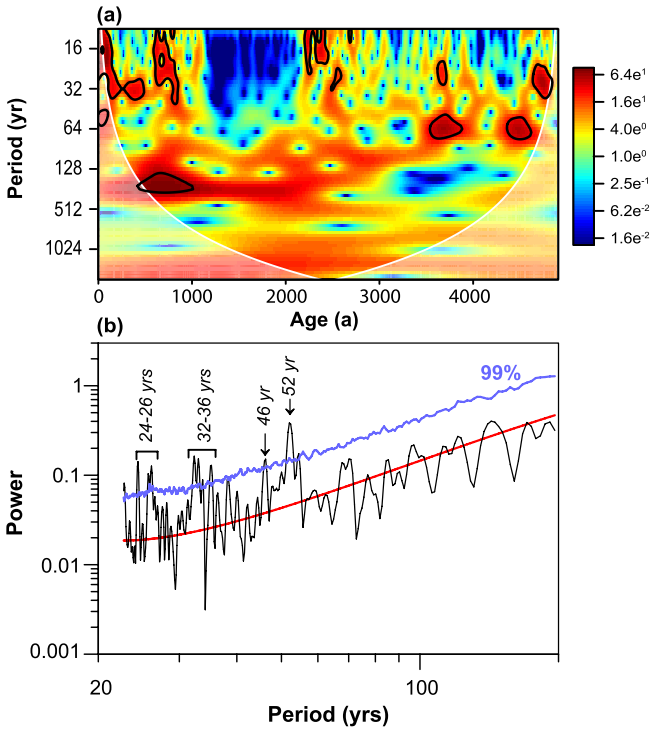

Figure 8. Spectral analysis of the detrended and non-interpolated ln(K/Al) record from Core M125-67-4 (black line). (a) Wavelet spectrum (black lines indicate 95% confidence), white shading denotes cone of influence); (b) power spectrum with 99% confidence interval based on Monte Carlo simulation (blue line) and red noise level (red line). The dominant periods are indicated.

Figure 8a). A cross-wavelet of ln(K/Al) of Core M125-67-4 and Sr/Ca of Botuverá likewise shows only short periods of significant coherence in the AMO band of ~60 years (around 4.3 and 0.9 ka; Figure S3). It hence appears that the discussed AMO impact on the SALLJ alone cannot fully explain the dipole-behavior of our records from Core M125-67-4 and Botuverá Cave. Indeed, this is expected as the Jequitinhonha catchment is not directly affected by the SALLJ, in contrast to Botuverá Cave (Jones & Carvalho, 2018). Nevertheless, the spurious presence of AMO-related periods in ln(K/Al) of Core M126-67-4 is consistent with similar observations in other paleo-precipitation records from eastern Brazil (Novello et al., 2012; Stríkis et al., 2011) and corroborates the view that AMO is an intrinsic component of SASM variability even under glacial boundary conditions (Chiessi et al., 2009). However, based on the available data, a comprehensive explanation of the spatiotemporal precipitation variability across eastern South America apparently requires the combined influence of the South Atlantic Dipole and the AMO, both driven by AMOC fluctuations.

The impact of relatively small-scale AMOC fluctuations across the late Holocene on the SAMS implies that South American climate is sensitive to high-latitude climate disturbances. Notably, this sensitivity increased over the past 2–3 kyrs particularly in eastern Brazil as a consequence of increasing austral summer insolation and the ensuing aridification. Enhanced meltwater input from shrinking Greenland glaciers as predicted for the next decades in response to global warming is likely to initiate a rapid AMOC decrease (Böning et al., 2016; IPCC, 2021) and therefore likely trigger a substantial weakening of the SACZ and intensification of the SALLJ. Such a scenario is alarming, as numerical models show that future global warming will lead to an enhanced moisture gradient between increasingly more arid eastern Brazil and wetter southeastern South America (IPCC, 2021). Hence, shifts in the precipitation distribution due to a weakened AMOC will further reduce rainfall amounts over already drought-prone eastern South America, but also increase the risk for torrential rainfall across southern parts of eastern Brazil, considerably elevating the eminent socio-economic pressure in both regions.

7. Conclusions

Our new record of mid to late Holocene precipitation variability over eastern Brazil reveals a high sensitivity to climate disturbances of high northern latitude origin that are transmitted into low latitudes via changes in AMOC strength. Resultant shifts in the oceanic surface heat distribution within the North and South Atlantic thereby alter the mean state of major climatic modes, that is, the South Atlantic Dipole and the AMO. The South Atlantic Dipole reinforces a dipole-like behavior between SACZ and SALLJ, which is amplified by the influence of the AMO on the SALLJ strength. In summary, phases of sluggish AMOC and cooling in the high latitude North Atlantic strengthens the SALLJ on the expense of the SACZ, leading to more aridity in eastern Brazil and more precipitation over southeastern South America. As global warming is predicted to lead to a weakened AMOC and reduced SACZ intensity, eastern Brazil will likely become more affected by severe droughts in the coming decades.

Data Availability Statement

All data published in this paper will be made available on the PANGAEA data base (https://doi.pangaea.de/10.1594/PANGAEA.930811).

Acknowledgments
The authors acknowledge support by Captain Hammacher and the crew of R/V METEOR during the M125 Expedition. Gregor Austermann and Ilse Glass provided support during XRD analyses, Andreas Koutsodendris assisted in XRF scanning. A. Bahr was supported by DFG grant BA3809/9, A. L. Albuquerque is a CNPq senior researcher (grant 302521/2017-8). C. Chiessi acknowledges financial support from FAPESP (grants 2018/15123-4 and 2019/24349-9), CAPES (grants 564/2015 and 88881.313535/2019-01), CNPq (grants 302607/2016-1 and 312458/2020-7), and the Alexander von Humboldt Foundation. E. Schefuß is funded through the DFG Research Center/Cluster of Excellence "The Ocean in the Earth System" at MARUM. F. Cruz acknowledges FAPESP grant 2017/50085-3. A. Jaeschke acknowledges financial support from DFG (grant 268236062—SFB 1211). S. Kaboth-Bahr acknowledges an Open-Topic Post-Doc Fellowship from the University of Potsdam. Open access funding enabled and organized by Projekt DEAL.

References

Alvares, C. A., Stape, J. L., Sentelhas, P. C., de Moraes, G., Leonardo, J., & Sparovek, G. (2013). Köppen's climate classification map for Brazil. *Meteorologische Zeitschrift*, *22*, 711–728. https://doi.org/10.1127/0941-2948/2013/0507

Alves, E., Macario, K., Souza, R., Pimenta, A., Douka, K., Oliveira, F., et al. (2015). Radiocarbon reservoir corrections on the Brazilian coast from pre-bomb marine shells. *Quaternary Geochronology*, *29*, 30–35. https://doi.org/10.1016/j.quageo.2015.05.006

Asmerom, Y., Baldini, J. U. L., Prufer, K. M., Polyak, V. J., Ridley, H. E., Aquino, V. V., et al. (2020). Intertropical convergence zone variability in the Neotropics during the Common Era. *Science Advances*, *6*, eaax3644. https://doi.org/10.1126/sciadv.aax3644

Bahr, A., Spadano Albuquerque, A., Ardenghi, N., Batenburg, S., Bayer, M., Catunda, M., et al. (2016). *South American hydrological balance and paleoceanography during the late Pleistocene and Holocene (SAMBA)–Cruise no. M125, March 21–April 15, 2016-Rio de Janeiro (Brazil)–Fortaleza (Brazil)*. DFG-Senatskommission für Ozeanographie. https://doi.org/10.2312/cr_m125

Baker, P. A., & Fritz, S. C. (2015). Nature and causes of Quaternary climate variation of tropical South America. *Quaternary Science Reviews*, *124*, 31–47. https://doi.org/10.1016/j.quascirev.2015.06.011

Baker, P. A., Fritz, S. C., Garland, J., & Ekdahl, E. (2005). Holocene hydrologic variation at Lake Titicaca, Bolivia/Peru, and its relationship to North Atlantic climate variation. *Journal of Quaternary Science: Published for the Quaternary Research Association*, *20*, 655–662. https://doi.org/10.1002/jqs.987

Bernal, J., Cruz, F. W., Stríkis, N. M., Wang, X., Deininger, M., Catunda, M. C. A., et al. (2016). High-resolution Holocene South American monsoon history recorded by a speleothem from Botuverá Cave, Brazil. *Earth and Planetary Science Letters*, *450*, 186–196. https://doi.org/10.1016/j.epsl.2016.06.008

Blaauw, M., & Christen, J. A. (2011). Flexible paleoclimate age-depth models using an autoregressive gamma process. *Bayesian analysis*, *6*, 457–474. https://doi.org/10.1214/ba/1339616472

Bombardi, R. J., Carvalho, L. M., Jones, C., & Reboita, M. S. (2014). Precipitation over eastern South America and the South Atlantic Sea surface temperature during neutral ENSO periods. *Climate Dynamics*, *42*, 1553–1568. https://doi.org/10.1007/s00382-013-1832-7

Böning, C. W., Behrens, E., Biastoch, A., Getzlaff, K., & Bamber, J. L. (2016). Emerging impact of Greenland meltwater on deepwater formation in the North Atlantic Ocean. *Nature Geoscience*, *9*, 523–527. https://doi.org/10.1038/ngeo2740

Broecker, W. (1998). Paleocean circulation during the last deglaciation: A bipolar seesaw? *Paleoceanography*, *13*, 119–121. https://doi.org/10.1029/97PA03707

Bush, R. T., & McInerney, F. A. (2013). Leaf wax n-alkane distributions in and across modern plants: Implications for paleoecology and chemotaxonomy. *Geochimica et Cosmochimica Acta*, *117*, 161–179. https://doi.org/10.1016/j.gca.2013.04.016

Cai, W., McPhaden, M. J., Grimm, A. M., Rodrigues, R. R., Taschetto, A. S., Garreaud, R. D., et al. (2020). Climate impacts of the El Niño–Southern Oscillation on South America. *Nature Reviews Earth & Environment*, *1*, 215–231. https://doi.org/10.1038/s43017-020-0040-3

Campos, J., Cruz, F., Ambrizzi, T., Deininger, M., Vuille, M., Novello, V., & Strikis, N. (2019). Coherent South American Monsoon variability during the last millennium revealed through high-resolution proxy records. *Geophysical Research Letters*, *46*, 8261–8270. https://doi.org/10.1029/2019gl082513

Carvalho, L. M. (2020). Assessing precipitation trends in the Americas with historical data: A review. *Wiley Interdisciplinary Reviews: Climate Change*, *11*, e627. https://doi.org/10.1002/wcc.627

Carvalho, L. M., Jones, C., & Liebmann, B. (2004). The South Atlantic Convergence Zone: Intensity, form, persistence, and relationships with intraseasonal to interannual activity and extreme rainfall. *Journal of Climate*, *17*, 88–108. https://doi.org/10.1175/1520-0442(2004)017<0088:TSACZI>2.0.CO;2

Chang, H. K., Gonçalves, R. D., Aggarwal, P. K., Stradioto, M. R., Hespanhol, E. C., Sturchio, N. C., et al. (2020). Groundwater isotope ratios reflect convective and stratiform (paleo) precipitation fractions in Brazil. *Journal of Hydrology*, *585*, 124801. https://doi.org/10.1016/j.jhydrol.2020.124801

Chang, P., Ji, L., & Li, H. (1997). A decadal climate variation in the tropical Atlantic Ocean from thermodynamic air-sea interactions. *Nature*, *385*(6616), 516–518. https://doi.org/10.1038/385516a0

Chiessi, C. M., Mulitza, S., Pätzold, J., Wefer, G., & Marengo, J. A. (2009). Possible impact of the Atlantic Multidecadal Oscillation on the South American summer monsoon. *Geophysical Research Letters*, *36*, L21707. https://doi.org/10.1029/2009GL039914

Chiessi, C. M., Mulitza, S., Taniguchi, N. K., Prange, M., Campos, M. C., Häggi, C., et al. (2021). Mid- to late Holocene contraction of the Intertropical Convergence Zone over northeastern South America. *Paleoceanography and Paleoclimatology*, *36*, e2020PA003936. https://doi.org/10.1029/2020PA003936

Coelho, C. A., de Oliveira, C. P., Ambrizzi, T., Reboita, M. S., Carpenedo, C. B., Campos, J. L. P. S., et al. (2016). The 2014 southeast Brazil austral summer drought: Regional scale mechanisms and teleconnections. *Climate Dynamics*, *46*, 3737–3752. https://doi.org/10.1007/s00382-015-2800-1

Conroy, J. L., Overpeck, J. T., & Cole, J. E. (2010). El Niño/Southern Oscillation and changes in the zonal gradient of tropical Pacific sea surface temperature over the last 1.2 ka. *PAGES News*, *18*, 32–34. https://doi.org/10.22498/pages.18.1.32

CPRM—Serviço Geológico do Brasil. (2003a). *Mapa geológico do estado da Bahia*. CPRM. Escala 1:1.000.000.

CPRM—Serviço Geológico do Brasil. (2003b). *Mapa geológico do estado de Minas Gerais*. CPRM. Escala 1:1.000.000.

Cruz, F. W., Burns, S. J., Jercinovic, M., Karmann, I., Sharp, W. D., & Vuille, M. (2007). Evidence of rainfall variations in Southern Brazil from trace element ratios (Mg/Ca and Sr/Ca) in a Late Pleistocene stalagmite. *Geochimica et Cosmochimica Acta*, *71*, 2250–2263. https://doi.org/10.1016/j.gca.2007.02.005

Cruz, F. W., Burns, S. J., Karmann, I., Sharp, W. D., Vuille, M., Cardoso, A. O., et al. (2005). Insolation-driven changes in atmospheric circulation over the past 116,000 years in subtropical Brazil. *Nature*, *434*, 63–66. https://doi.org/10.1038/nature03365

Cruz, F. W., Vuille, M., Burns, S. J., Wang, X., Cheng, H., Werner, M., et al. (2009). Orbitally driven east-west antiphasing of South American precipitation. *Nature Geoscience*, *2*, 210–214. https://doi.org/10.1038/ngeo444

Dansgaard, W. (1964). Stable isotopes in precipitation. *Tellus*, *16*, 436–468. https://doi.org/10.3402/tellusa.v16i4.8993

Deininger, M., Ward, B. M., Novello, V. F., & Cruz, F. W. (2019). Late Quaternary variations in the South American Monsoon System as inferred by speleothems—New perspectives using the SISAL Database. *Quaternary*, *2*, 6. https://doi.org/10.3390/quat2010006

Diefendorf, A. F., & Freimuth, E. J. (2017). Extracting the most from terrestrial plant-derived n-alkyl lipids and their carbon isotopes from the sedimentary record: A review. *Organic Geochemistry*, *103*, 1–21. https://doi.org/10.1016/j.orggeochem.2016.10.016

dos Santos, V., Gastmans, D., Sánchez-Murillo, R., Gozzo, L. F., Batista, L. V., Manzione, R. L., & Martinez, J. (2019). Regional atmospheric dynamics govern interannual and seasonal stable isotope composition in southeastern Brazil. *Journal of Hydrology*, *579*, 124136. https://doi.org/10.1016/j.jhydrol.2019.124136

Eglinton, G., & Hamilton, R. L. (1967). Leaf epicuticular waxes. *Science*, *156*, 1322–1335. https://doi.org/10.1126/science.156.3780.1322

Erfanian, A., Wang, G., & Fomenko, L. (2017). Unprecedented drought over tropical South America in 2016: Significantly under-predicted by tropical SST. *Scientific Reports*, *7*, 5811. https://doi.org/10.1038/s41598-017-05373-2

Gouhier, T. C., Grinsted, A., & Simko, V. (2019). *R package biwavelet: Conduct univariate and bivariate wavelet analyses (version 0.20.19)*. Retrieved from https://github.com/tgouhier/biwavelet

Grimm, A. M. (2003). The El Niño impact on the summer monsoon in Brazil: Regional processes versus remote influences. *Journal of Climate*, *16*, 263–280. https://doi.org/10.1175/1520-0442(2003)016<0263:TENIOT>2.0.CO;2

Grimm, A. M. (2011). Interannual climate variability in South America: Impacts on seasonal precipitation, extreme events, and possible effects of climate change. *Stochastic Environmental Research and Risk Assessment*, *25*, 537–554. https://doi.org/10.1007/s00477-010-0420-1

Grimm, A. M., & Tedeschi, R. G. (2009). ENSO and extreme rainfall events in South America. *Journal of Climate*, *22*, 1589–1609. https://doi.org/10.1175/2008JCLI2429.1

Hammer, Ø., Harper, D. A. T., & Ryan, P. D. (2001). PAST: Paleontological statistics software package for education and data analysis. *Palaeontologia Electronica*, *4*, 9.

Hou, A., Bahr, A., Raddatz, J., Voigt, S., Greule, M., Albuquerque, A. L., et al. (2020). Insolation and greenhouse gas forcing of the South American Monsoon System across three Glacial-Interglacial cycles. *Geophysical Research Letters*, *47*, e2020GL087948. https://doi.org/10.1029/2020gl087948

Hou, A., Bahr, A., Schmidt, S., Strebl, C., Albuquerque, A. L., Chiessi, C. M., & Friedrich, O. (2020). Forcing of western tropical South Atlantic sea surface temperature across three glacial-interglacial cycles. *Global and Planetary Change*, *188*, 103150. https://doi.org/10.1016/j.gloplacha.2020.103150

Hunt, J. D., Stilpen, D., & de Freitas, M. A. V. (2018). A review of the causes, impacts and solutions for electricity supply crises in Brazil. *Renewable and Sustainable Energy Reviews*, *88*, 208–222. https://doi.org/10.1016/j.rser.2018.02.030

IPCC. (2021). *Climate change 2021: The physical science basis. Contribution of working group I to the sixth assessment report of the intergovernmental panel on climate change*. Cambridge University Press.

Jones, C., & Carvalho, L. M. (2018). The influence of the Atlantic multidecadal oscillation on the eastern Andes low-level jet and precipitation in South America. *npj Climate and Atmospheric Science*, *1*, 40. https://doi.org/10.1038/s41612-018-0050-8

Kahmen, A., Hoffmann, B., Schefuß, E., Arndt, S. K., Cernusak, L. A., West, J. B., & Sachse, D. (2013). Leaf water deuterium enrichment shapes leaf wax n-alkane δD values of angiosperm plants II: Observational evidence and global implications. *Geochimica et Cosmochimica Acta*, *111*, 50–63. https://doi.org/10.1016/j.gca.2012.09.004

Kahmen, A., Schefuß, E., & Sachse, D. (2013). Leaf water deuterium enrichment shapes leaf wax n-alkane δD values of angiosperm plants I: Experimental evidence and mechanistic insights. *Geochimica et Cosmochimica Acta*, *111*, 39–49. https://doi.org/10.1016/j.gca.2012.09.003

Kissel, C., Van Toer, A., Laj, C., Cortijo, E., & Michel, E. (2013). Variations in the strength of the North Atlantic bottom water during Holocene. *Earth and Planetary Science Letters*, *369–370*, 248–259. https://doi.org/10.1016/j.epsl.2013.03.042

Laskar, J., Robutel, P., Joutel, F., Gastineau, M., Correia, A., & Levrard, B. (2004). A long-term numerical solution for the insolation quantities of the Earth. *Astronomy & Astrophysics*, *428*, 261–285. https://doi.org/10.1051/0004-6361:20041335

Liebmann, B., Kiladis, G. N., Vera, C. S., Saulo, A. C., & Carvalho, L. M. (2004). Subseasonal variations of rainfall in South America in the vicinity of the low-level jet east of the Andes and comparison to those in the South Atlantic convergence zone. *Journal of Climate*, *17*, 3829–3842. https://doi.org/10.1175/1520-0442(2004)017<3829:SVORIS>2.0.CO;2

Mann, M. E., Zhang, Z., Rutherford, S., Bradley, R. S., Hughes, M. K., Shindell, D., et al. (2009). Global signatures and dynamical origins of the Little Ice Age and Medieval Climate Anomaly. *Science*, *326*, 1256–1260. https://doi.org/10.1126/science.1177303

Marcello, F., Wainer, I., Gent, P. R., Otto-Bliesner, B. L., & Brady, E. C. (2019). South Atlantic surface boundary current system during the last millennium in the CESM-LME: The medieval climate anomaly and little ice age. *Geosciences*, *9*, 299. https://doi.org/10.3390/geosciences9070299

Marengo, J. A., & Bernasconi, M. (2015). Regional differences in aridity/drought conditions over Northeast Brazil: Present state and future projections. *Climatic Change*, *129*, 103–115. https://doi.org/10.1007/s10584-014-1310-1

Marengo, J. A., Torres, R. R., & Alves, L. M. (2017). Drought in Northeast Brazil—Past, present, and future. *Theoretical and Applied Climatology*, *129*, 1189–1200. https://doi.org/10.1007/s00704-016-1840-8

Meyers, S. (2014). *Astrochron: An R package for astrochronology*. Retrieved from http:org/web/packages/astrochron/index.html

Novello, V. F., Cruz, F. W., Karmann, I., Burns, S. J., Stríkis, N. M., Vuille, M., et al. (2012). Multidecadal climate variability in Brazil's Nordeste during the last 3000 years based on speleothem isotope records. *Geophysical Research Letters*, *39*. https://doi.org/10.1029/2012GL053936

Novello, V. F., Cruz, F. W., Moquet, J., Vuille, M., de Paula, M., Nunes, D., et al. (2018). Two millennia of South Atlantic Convergence Zone variability reconstructed from isotopic proxies. *Geophysical Research Letters*, *45*, 5045–5051. https://doi.org/10.1029/2017GL076838

Parsons, L. A., Yin, J., Overpeck, J. T., Stouffer, R. J., & Malyshev, S. (2014). Influence of the Atlantic Meridional Overturning Circulation on the monsoon rainfall and carbon balance of the American tropics. *Geophysical Research Letters*, *41*(1), 146–151. https://doi.org/10.1002/2013GL058454

Ribeiro, M. C., Metzger, J. P., Martensen, A. C., Ponzoni, F. J., & Hirota, M. M. (2009). The Brazilian Atlantic Forest: How much is left, and how is the remaining forest distributed? Implications for conservation. *Biological Conservation*, *142*, 1141–1153. https://doi.org/10.1016/j.biocon.2009.02.021

Rojas, M., Arias, P. A., Flores-Aqueveque, V., Seth, A., & Vuille, M. (2016). The South American monsoon variability over the last millennium in climate models. *Climate of the Past*, *12*, 1681–1691. https://doi.org/10.5194/cp-12-1681-2016

Sachs, J. P. (2007). Cooling of Northwest Atlantic slope waters during the Holocene. *Geophysical Research Letters*, *34*, L03609. https://doi.org/10.1029/2006GL028495

Sachse, D., Billault, I., Bowen, G. J., Chikaraishi, Y., Dawson, T. E., Feakins, S. J., et al. (2012). Molecular paleohydrology: Interpreting the hydrogen-isotopic composition of lipid biomarkers from photosynthesizing organisms. *Annual Review of Earth and Planetary Sciences*, *40*, 221–249. https://doi.org/10.1146/annurev-earth-042711-105535

Schefuß, E., Schouten, S., & Schneider, R. R. (2005). Climatic controls on central African hydrology during the past 20,000 years. *Nature*, *437*, 1003–1006. https://doi.org/10.1038/nature03945

Schulz, M., & Mudelsee, M. (2002). REDFIT: Estimating red-noise spectra directly from unevenly spaced paleoclimatic time series. *Computers & Geosciences*, *28*, 421–426. https://doi.org/10.1016/S0098-3004(01)00044-9

Seidov, D., & Maslin, M. (2001). Atlantic Ocean heat piracy and the bipolar climate see-saw during Heinrich and Dansgaard–Oeschger events. *Journal of Quaternary Science*, *16*, 321–328. https://doi.org/10.1002/jqs.595

Sierra, J. P., Arias, P. A., & Vieira, S. C. (2015). Precipitation over Northern South America and its seasonal variability as simulated by the CMIP5 models. *Advances in Meteorology*, *2015*, 1–22. https://doi.org/10.1155/2015/634720

Siongco, A. C., Hohenegger, C., & Stevens, B. (2014). The Atlantic ITCZ bias in CMIP5 models. *Climate Dynamics*, *45*, 1169–1180. https://doi.org/10.1007/s00382-014-2366-3

Stríkis, N. M., Cruz, F. W., Cheng, H., Karmann, I., Edwards, R. L., Vuille, M., et al. (2011). Abrupt variations in South American monsoon rainfall during the Holocene based on a speleothem record from central-eastern Brazil. *Geology*, *39*, 1075–1078. https://doi.org/10.1130/g32098.1

Stuiver, M., Reimer, P., & Reimer, R. (2020). *CALIB 8.2*. Retrieved from http://calib.org/calib/

Thornalley, D. J., Oppo, D. W., Ortega, P., Robson, J. I., Brierley, C. M., Davis, R., et al. (2018). Anomalously weak Labrador Sea convection and Atlantic overturning during the past 150 years. *Nature*, *556*, 227–230. https://doi.org/10.1038/s41586-018-0007-4

Tian, J., Xie, X., Ma, W., Jin, H., & Wang, P. (2011). X-ray fluorescence core scanning records of chemical weathering and monsoon evolution over the past 5 Myr in the southern South China Sea. *Paleoceanography*, *26*, PA4202. https://doi.org/10.1029/2010pa002045

Tintelnot, M. (1995). *Transport and deposition of fine-grained sediments on the Brazilian continental shelf as revealed by clay mineral distribution* (PhD Thesis). Heidelberg University.

Tomasella, J., Sene Gonçalves, A., Schneider Falck, A., Oliveira Caram, R., Rodrigues Diniz, F. L., Rodriguez, D. A., et al. (2019). Probabilistic flood forecasting in the Doce Basin in Brazil: Effects of the basin scale and orientation and the spatial distribution of rainfall. *Journal of Flood Risk Management*, *12*, e12452. https://doi.org/10.1111/jfr3.12452

Utida, G., Cruz, F. W., Etourneau, J., Bouloubassi, I., Schefuß, E., Vuille, M., et al. (2019). Tropical South Atlantic influence on Northeastern Brazil precipitation and ITCZ displacement during the past 2300 years. *Scientific Reports*, *9*, 1698. https://doi.org/10.1038/s41598-018-38003-6

Venegas, S., Mysak, L., & Straub, D. (1997). Atmosphere–ocean coupled variability in the South Atlantic. *Journal of Climate*, *10*, 2904–2920. https://doi.org/10.1175/1520-0442(1997)010<2904:AOCVIT>2.0.CO;2

Vera, C., Higgins, W., Amador, J., Ambrizzi, T., Garreaud, R., Gochis, D., et al. (2006). Toward a unified view of the American monsoon systems. *Journal of Climate*, *19*, 4977–5000. https://doi.org/10.1175/JCLI3896.1

Vuille, M., Burns, S., Taylor, B., Cruz, F., Bird, B., Abbott, M., et al. (2012). A review of the South American monsoon history as recorded in stable isotopic proxies over the past two millennia. *Climate of the Past*, *8*, 1309–1321. https://doi.org/10.5194/cp-8-1309-2012

Wainer, I., Prado, L. F., Khodri, M., & Otto-Bliesner, B. (2014). Reconstruction of the South Atlantic Subtropical Dipole index for the past 12,000 years from surface temperature proxy. *Scientific Reports*, *4*, 1–8. https://doi.org/10.1038/srep05291

Wainer, I., Prado, L. F., Khodri, M., & Otto-Bliesner, B. (2021). The South Atlantic sub-tropical dipole mode since the last deglaciation and changes in rainfall. *Climate Dynamics*, *56*, 109–122. https://doi.org/10.1007/s00382-020-05468-z

Xie, P., & Arkin, P. A. (1997). Global precipitation: A 17-year monthly analysis based on gauge observations, satellite estimates, and numerical model outputs. *Bulletin of the American Meteorological Society*, *78*, 2539–2558. https://doi.org/10.1175/1520-0477(1997)078<2539:GPAYMA>2.0.CO;2

Yarincik, K., Murray, R., & Peterson, L. (2000). Climatically sensitive eolian and hemipelagic deposition in the Cariaco Basin, Venezuela, over the past 578,000 years: Results from Al/Ti and K/Al. *Paleoceanography and Paleoclimatology*, *15*, 210–228. https://doi.org/10.1029/1999PA900048

Zabel, M., Schneider, R. R., Wagner, T., Adegbie, A. T., de Vries, U., & Kolonic, S. (2001). Late Quaternary climate changes in Central Africa as inferred from terrigenous input to the Niger Fan. *Quaternary Research*, *56*, 207–217. https://doi.org/10.1006/qres.2001.2261